RESONANT PRODUCTION OF SPIN-3/2 COLOR OCTET ELECTRON AT THE LHeC*

M. Sahin

Department of Physics, Usak University, Usak, Turkey
mehmet.sahin@usak.edu.tr

In this work, we investigate resonant production of spin-3/2 color octet electron at the Large Hadron electron Collider (LHeC). Signal and background analysis are performed and discovery, observation and exclusion limits are determined for spin 3/2 color octet electron masses. Reachable values of the compositeness scale are presented as a function of the spin-3/2 color octet electron masses.

1. Introduction

The Standard Model (SM) of particle physics successfully explains electromagnetic, weak and strong interactions of fundamental particles. The SM predictions are consistent with numerous experiments. Furthermore, results of the ATLAS and the CMS collaborations [1, 2] are consistent with the SM Higgs boson hypothesis. If the new particle is the SM Higgs boson, why the fundamental particles have mass is explained by SM. However, SM does not explain some cases such as quark–lepton symmetry, family replication, hierarchy problems, charge quantization, *etc.* Many theoretical hypothesis are proposed to clarify these cases. Supersymmetry (SUSY), extra dimensions, grand unified theories (GUTs) and compositeness seem to be most promising candidates for beyond the SM physics.

The subjects of family replication and quark–lepton symmetry are explained in the best manner by compositeness. In the framework of composite models, quarks, leptons and gauge bosons are composite particles made up of more basic constituents. These basic constituents are named preons. The preonic models lead to a rich spectrum of new type particles such as diquarks, leptoquarks, leptogluons, dileptons and excited fermions, *etc.*

We are interested in color octet leptons which are predicted in all composite models with colored preons [3–9]. For example, according to fermion–scalar models [9], a bound state of one fermionic preon and one scalar antipreon would produce leptons $l = (F\bar{S}) = 1 \oplus 8$, where F and S are color triplet preons. Therefore, each SM lepton is considered to be accompanied by its own color octet partner. Color octet electrons which are also called leptogluons, have the same status as the excited leptons so, as the excited leptons, they have a spin of $1/2$ or $3/2$. The motivation for spin-$3/2$ leptons comes from composite models [10, 11] and supergravity gauge theories [12]. The spin-$1/2$ color octet electron was investigated in earlier papers [9, 13–17]. Recently, the spin-$1/2$ color octet electron has been analyzed for future high energy colliders: Large Hadron electron Collider (LHeC) [18], International Linear Collider (ILC) and Compact Linear Collider (CLIC) [19], and Large Hadron Collider (LHC) [20]. Although the spin-$3/2$ color octet electron is mentioned in literature, it has not been investigated in details up to now. In order to close this gap in the literature, we investigate resonant production of the spin-$3/2$ color octet electron at the LHeC.

LHeC project supported by CERN, ECFA and NuPECC is a new LHC based electron–proton and electron–ion collider [21]. LHeC is under design for synchronous operation with the LHC at CERN in the twenties. Conceptual design report (CDR) of the LHeC was completed and published in summer 2012 [22]. The CDR of the LHeC describes two options for the LHeC, a ring–ring (RR) and a linac–ring (LR) configurations. After the CDR was completed, it was decided to continue the technical design work for the linac–ring (LR) configuration in a recent workshop [23, 24]. History and status of linac–ring type collider proposals can be found in review [25]. We have preferred two energy options of linac–ring (LR) type LHeC in our calculations. The first one is a lower-energy LHeC ERL option (see LHeC CDR [22] Section 7.1.2). In this option, the lepton beam energy is 60 GeV and proton beam energy is 7000 GeV. Electron–proton luminosity is 10^{33} cm^{-2}s^{-1}. The second option is a higher-energy LHeC ERL option (see LHeC CDR [22] Section 7.1.5). In this case, the lepton beam energy is 150 GeV and proton beam energy is 7000 GeV. Electron–proton luminosity is 10^{35} cm^{-2}s^{-1}. These properties of LHeC are shown in Table I.

TABLE I

Tentative parameters of the LHeC linac–ring options. ERL denotes energy recovery linac.

Stage	E_e [GeV]	$\sqrt{s}$ [TeV]	L [10^{33} cm^{-2}s^{-1}]
Lower-energy LHeC ERL (LHeC-1)	60	1.296	1
Higher-energy LHeC ERL (LHeC-2)	150	2.049	100

Spin-3/2 color octet electron could be produced as pair, single and indirectly at the LHC such as the spin-1/2 color octet electron [20]. Pair production of spin-3/2 color octet is almost independent of compositeness scale (Λ) at the LHC. Therefore, we could not put strong limitations on compositeness scale (Λ) for the pair produced spin-3/2 color octet electron at the LHC. In the case of the single production of the spin-1/2 and spin-3/2 color octet electrons at the LHC, single production cross sections scale as $1/\Lambda^2$ for the spin-1/2 [19] and $1/\Lambda^4$ for spin-3/2 color octet electrons. So, the cross section values of the single produced spin-3/2 color octet electron are much smaller than the single produced spin-1/2 color octet electron's cross section values at the LHC. Thus, the single production of spin-3/2 color octet electron at the LHC is not so useful to probe high values of compositeness scale at the LHC. Similar arguments are valid for indirect production of color octet electrons (a t-channel exchange of spin-3/2 color octet electron) at the LHC [19, 20], since the cross sections are proportional to $1/\Lambda^2$ and $1/\Lambda^4$ for spin-1/2 and spin-3/2 color octet electrons respectively. Due to all these reasons, compositeness scale for the spin-3/2 color octet electron will be probed in the best manner by the LHeC (see Sections 3 and 4).

It should be mentioned that first generation leptoquark (decaying to eq) has the similar signatures as first generation of color octet electrons (decaying to eg), since both quarks and gluons will be seen as a jet in the detector. Hence, we compare properties of these particles (leptoquarks and leptogluons) and their phenomenology in this study. Leptoquarks are color triplet bosons which carry fractional electric charge ($Q = \pm 1/3, \pm 2/3, \pm 4/3, \pm 5/3$). They could be either scalar or vector particles. Leptoquarks couple directly to leptons and quarks. Three generations of leptoquarks are predicted. On the other hand, leptogluons are color octet fermions which carry unit electric charge. They could be either spin-1/2 or spin-3/2 particles. Leptogluons couple directly to leptons and gluons. Three generations of leptogluons are predicted. Their spin and charge quantum numbers make differences between leptoquarks and leptogluons. Like scalar and vector leptoquarks, spin-1/2 and spin-3/2 leptogluons have different spin quantum numbers that explains why their angular distributions are different (see Sections 3.1 and 3.2). Although leptoquarks and leptogluons have the same final state in detector, we can differentiate them because they have different spin and charge quantum numbers. Moreover, they have different cross section values because their interactions with leptons, quarks and gluons are different. Therefore, we do not use the same experimental bounds for scalar leptoquarks, vector leptoquarks, spin-1/2 leptogluons and spin-3/2 leptogluons. There are existing experimental bounds on leptoquarks (see ATLAS and CMS exotictwiki page [26, 27]). Although ATLAS and CMS data of LHC search of

leptoquarks (decaying to charged leptons and quarks) can be used as approximate bounds for leptogluons, there are no published results of ATLAS and CMS for spin-3/2 color octet electron.

In this paper, we consider resonant production of spin-3/2 color octet electron (e_8) at the Large Hadron electron Collider. In Section 2, the interaction Lagrangian of spin-3/2 leptogluons, decay widths and resonant production cross sections of spin-3/2 color octet electron at different stages of the LHeC are presented. In Section 3, signal and background analysis are performed at the LHeC, and achievable masses and compositeness scale are determined for the spin-3/2 color octet electron. Finally, we give concluding remarks in Section 4.

2. Interaction Lagrangian, decay width and cross sections

For the interaction of spin-3/2 leptogluons with corresponding lepton and gluon, we use the following Lagrangian

$$L = \frac{1}{\Lambda^2} \sum_l \left\{ \bar{l}_{8\lambda}^\alpha \, g_s \, \partial^\lambda G_{\mu\nu}^\alpha \, \sigma^{\mu\nu} \left(\eta_{\rm L} l_{\rm L} + \eta_{\rm R} l_{\rm R} \right) \right\} + \text{h.c.} \,, \qquad (1)$$

where $\bar{l}_{8\lambda}^\alpha$ is a Rarita–Schwinger vector spinor [28] field for spin-3/2 leptogluons, index $\alpha = 1, 2, \ldots, 8$ denotes color, g_s is gauge coupling, $G_{\mu\nu}^\alpha$ is the field strength tensor for gluon, $\sigma^{\mu\nu}$ is the anti-symmetric tensor, $\eta_{\rm L}$ and $\eta_{\rm R}$ are the chirality factors, $l_{\rm L}$ and $l_{\rm R}$ represent left and right spinor components of leptons, and Λ is the compositeness scale. In this article, we introduce only the first family leptogluons. We assume that the leptogluons of the first family will be lighter than the others following what we observe experimentally in SM. The leptonic chirality conservation requires $\eta_{\rm L}\eta_{\rm R} = 0$. Therefore, we set $\eta_{\rm L} = 1$ and $\eta_{\rm R} = 0$ in our calculations.

Decay width of spin-3/2 color octet electron is given by

$$\Gamma_{e_8} = \frac{\alpha_{\rm s} M_{e_8}^5}{12 \Lambda^4} \,. \qquad (2)$$

The analytic expression for partonic level differential cross section for the process $e^- p \to e_8 \to g e^-$ is given by

$$\frac{d\hat{\sigma}}{d\hat{t}}(e^- p \to e_8 \to g e^-) = -\frac{64\alpha_{\rm s}^2 \hat{s}\hat{t} \left(\frac{\hat{s}^2}{M_{e_8}^2} - 3\left(\hat{s} + \hat{t}\right) \right)^2 \pi}{\alpha_{\rm s}^2 M_{e_8}^{12} + 144\Lambda^8 \left(M_{e_8}^2 - \hat{s} \right)^2} \,, \qquad (3)$$

where $\hat{s}$ and $\hat{t}$ are Mandelsam variables, $\alpha_{\rm s}$ is strong coupling constant and $\hat{\sigma}$ is partonic cross section.

For the numerical calculations, we implement the Lagrangian (see Eq. (1)) into the CALCHEP program [29, 30]. Figure 1 presents decay widths of the spin-3/2 color octet electron for $\Lambda = M_{e_8}$, $\Lambda = 5$ TeV and $\Lambda = 10$ TeV.
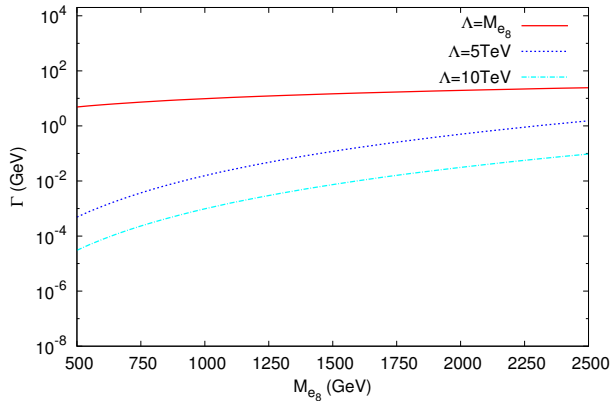

Fig. 1. The spin-3/2 color octet electron decay widths via its mass for $\Lambda = M_{e_8}$, $\Lambda = 5$ TeV and $\Lambda = 10$ TeV.

Resonant production cross sections of the spin-3/2 color octet electron for the two stages of the LHeC that are presented in Table I, are calculated using CALCHEP with CTEQ6L [31] parton distribution functions. In these calculations, we used factorization scale $Q^2 = M_{e_8}^2$. Figure 2 presents the resonant production cross sections of spin-3/2 color octet electron for $\Lambda = M_{e_8}$, $\Lambda = 5$ TeV and $\Lambda = 10$ TeV at the LHeC-1 with $\sqrt{s} = 1.296$ TeV. It is seen from Fig. 2 that spin-3/2 color octet electron has sufficiently high cross section values for $\Lambda = M_{e_8}$ and $\Lambda = 5$ TeV even at the high mass

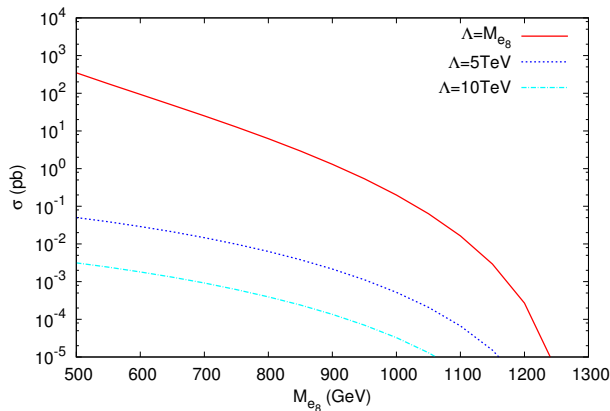Fig. 2. The resonant production of the spin-3/2 color octet electron at the LHeC-1 with $\sqrt{s} = 1.296$ TeV.

values of e_8. Figure 3 shows the resonant production cross sections of the spin-3/2 color octet electron for $\Lambda = M_{e_8}$, $\Lambda = 5$ TeV and $\Lambda = 10$ TeV at the LHeC-2 with $\sqrt{s} = 2.049$ TeV. It is seen from Fig. 3 that spin-3/2 color octet electron has sufficiently high cross sections for $\Lambda = M_{e_8}$, $\Lambda = 5$ TeV, and $\Lambda = 10$ TeV at the high mass values of e_8.
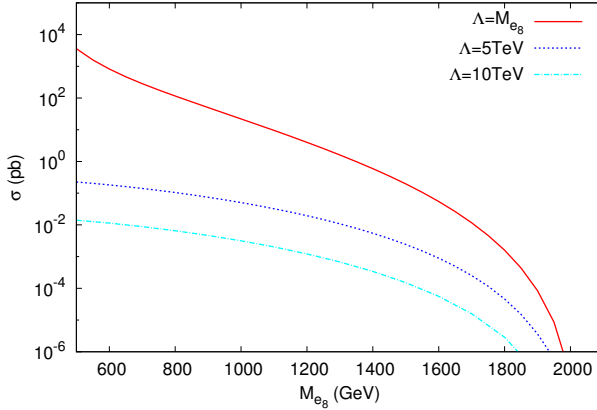

Fig. 3. The resonant production of the spin-3/2 color octet electron at the LHeC-2 with $\sqrt{s} = 2.049$ TeV.

3. Signal and background analysis

3.1. Lower-energy LHeC ERL stage
(LHeC-1 with $\sqrt{s} = 1.296$ TeV and $L_{int} = 10$ fb^{-1})

The center-of-mass energy of this LHeC option is 1.296 TeV and integrated luminosity is $L_{\mathrm{int}} = 10$ fb^{-1}. Our signal process is $ep \rightarrow e_8 \rightarrow eg + X$ and background process is $ep \rightarrow ej + X$ through γ and Z exchange, where g denotes gluon and j represents jet which is composed of quarks (u, $\bar{u}$, d, $\bar{d}$, c, $\bar{c}$, s, $\bar{s}$, b, $\bar{b}$) for background. In order to determine appropriate cuts, we need transverse momentum (P_{T}) and pseudo-rapidity (η) distributions of signal and background processes.

Figure 4 presents normalized transverse momentum distributions of final state jet for signal with $\Lambda = 5$ TeV in the left panel and signal with $\Lambda = M_{e_8}$ in the right panel, and also background for both panels. The final state electron's normalized transverse momentum distributions are the same as the plots of the final state jet in Fig. 4. It is seen from Fig. 4 that $P_{\mathrm{T}} > 50$ GeV cut for both final states (jet and electron final states) essentially reduces the background but the signal is almost unchanged. Left and right panels in Fig. 5 represent normalized pseudo-rapidity (η) distributions of electron for signal with $\Lambda = 5$ TeV and signal with $\Lambda = M_{e_8}$, and also for background,
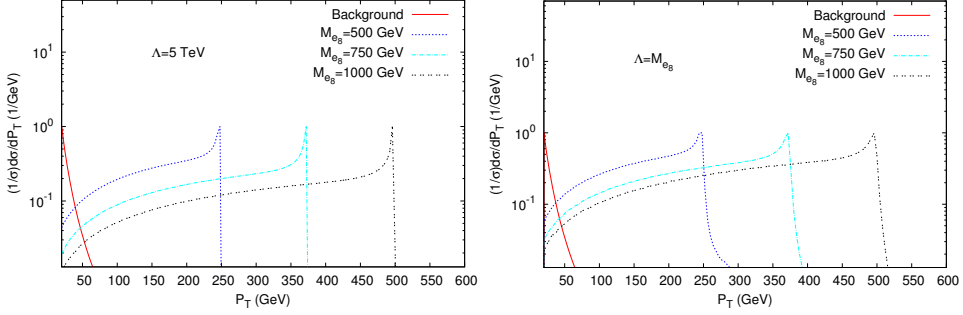
Fig. 4. Left: Normalized transverse momentum (P_T) distributions of final state jet for signal with $\Lambda = 5$ TeV and background at the LHeC-1 with $\sqrt{s} = 1.296$ TeV. Right: Normalized transverse momentum (P_T) distributions of final state jet for signal with $\Lambda = M_{e_8}$ TeV and background at the LHeC-1 with $\sqrt{s} = 1.296$ TeV.
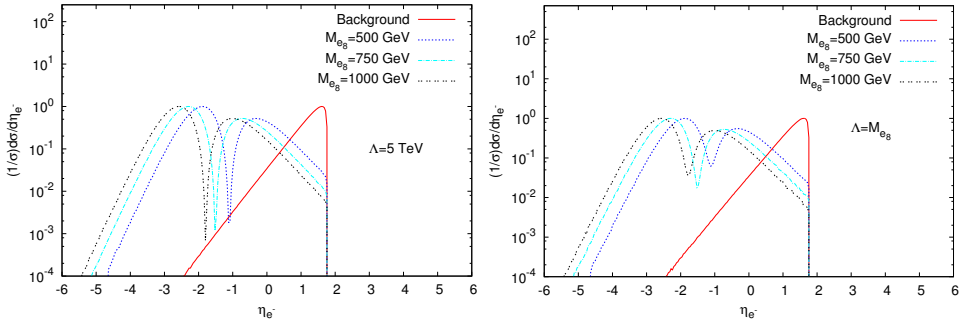

Fig. 5. Left: Normalized pseudo-rapidity distributions of final state electron for signal with $\Lambda = 5$ TeV and background at the LHeC-1 with $\sqrt{s} = 1.296$ TeV. Right: Normalized pseudo-rapidity distributions of final state electron for signal with $\Lambda = M_{e_8}$ and background at the LHeC-1 with $\sqrt{s} = 1.296$ TeV.

respectively. It is seen from left and right panels of Fig. 5 that η_{e^-} distributions of signal are drastically different from η_{e^-} distributions of background. In addition, most of background lie in $0 < \eta_{e^-} < 2$ region for both panels in Fig. 5. Left and right panels in Fig. 6 present normalized pseudo-rapidity (η) distributions of jet for signal with $\Lambda = 5$ TeV in the left panel and signal with $\Lambda = M_{e_8}$ in the right panel, and also for background (both panels), respectively. In Fig. 6, η_j distributions for signal and background are not drastically different. For this reason, we select pseudo-rapidity cuts values as follows: $-4 < \eta_{e^-} < -0.8$ for final state electron and $-4 < \eta_j < 1.5$ for final state jet. We present the invariant mass distributions for signal with $\Lambda = 5$ TeV in the left panel and signal $\Lambda = M_{e_8}$ in the right panel, and also for background (both panels) in Fig. 7.
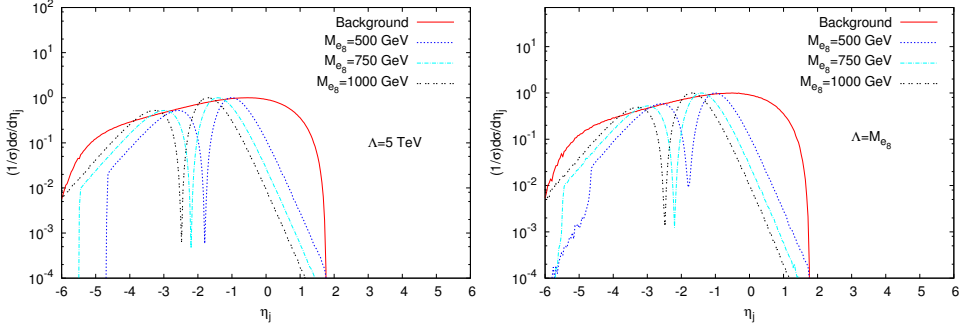
Fig. 6. Left: Normalized pseudo-rapidity distributions of final state jet for signal with $\Lambda = 5$ TeV and background at the LHeC-1 with $\sqrt{s} = 1.296$ TeV. Right: Normalized pseudo-rapidity distributions of final state jet for signal with $\Lambda = M_{e_8}$ TeV and background at the LHeC-1 with $\sqrt{s} = 1.296$ TeV.
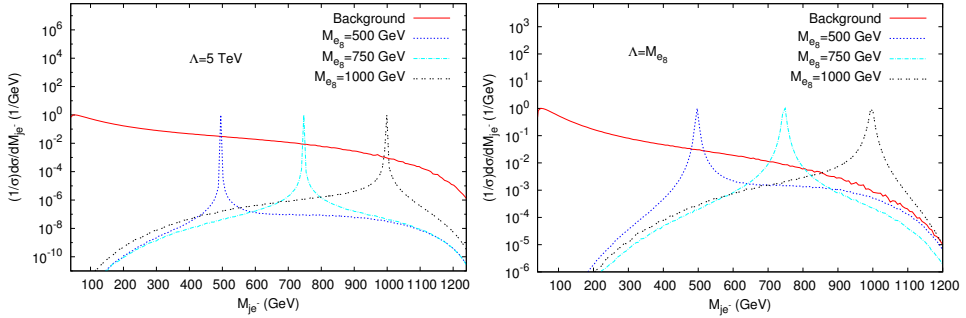

Fig. 7. Left: Normalized invariant mass distributions for signal with $\Lambda = 5$ TeV and background at the LHeC-1 with $\sqrt{s} = 1.296$ TeV. Right: Normalized invariant mass distributions for signal with $\Lambda = M_{e_8}$ and background at the LHeC-1 with $\sqrt{s} = 1.296$ TeV.

In order to extract the spin-3/2 color octet electron (e_8) signals (for the $\Lambda = 5$ TeV and $\Lambda = M_{e_8}$) and to suppress the backgrounds, we used $P_T > 50$ GeV for all final state electron and jet (these cut values are determined by Fig. 4), $-4 < \eta_{e^-} < -0.8$ for final state electron and $-4 < \eta_j < 1.5$ for final state jet (these cut values are determined by Figs. 5 and 6). In addition to these cut values, we used mass window as $M_{e_8} - 10$ GeV $< M_{je^-} < M_{e_8} + 10$ GeV for signal with $\Lambda = 5$ TeV and for background. It is seen from Fig. 1 that signal decay width values are quite small compared to 10 GeV when the $\Lambda = 5$ TeV. We also used mass window as $M_{e_8} - 20$ GeV $< M_{je^-} < M_{e_8} + 20$ GeV for signal with $\Lambda = M_{e_8}$ and background. As it is seen from Fig. 1, signal decay width values approximately are 10 GeV at the LHeC-1 kinematic limit (1296 GeV) when $\Lambda = M_{e_8}$.

By using a set of cuts that is mentioned above and $L_{\text{int}} = 10$ fb^{-1} integrated luminosity values of the LHeC-1, we have calculated event numbers for some mass values of e_8 and background. We present these event numbers in Table II.

TABLE II

The number of signal and background events for the LHeC-1 with $L_{\text{int}} = 10$ fb^{-1}. Here, N_{s} is a number of signal events and N_{b} is a number of background events.

M_{e_8} [GeV]	$\Lambda = 5$ TeV		$\Lambda = M_{e_8}$	
	N_{s}	N_{b}	N_{s}	N_{b}
500	304	1268	3559200	2538
600	185	838	1053100	1678
700	100	514	308510	1028
800	45	279	82767	558
900	16	126	18617	252
1000	4	43	3066	86
1100	—	9	278	18
1200	—	—	6	1

For statistical significance, we use the following formula [32]

$$S = \sqrt{2\left[(N_{\text{s}} + N_{\text{b}})\ln\left(1 + \frac{N_{\text{s}}}{N_{\text{b}}}\right) - N_{\text{s}}\right]}, \tag{4}$$

where N_{s} and N_{b} represent the number of signal and background events, respectively. The statistical significances of spin-3/2 color octet electron signal with $\Lambda = 5$ TeV are shown in Fig. 8 for the LHeC-1 with $\sqrt{s} = 1.296$ TeV and $L_{\text{int}} = 10$ fb^{-1}.

It is seen from Fig. 8 that upper mass limit for discovery (5σ) of spin-3/2 color octet electron (e_8) is 660 GeV at the LHeC-1 with $\sqrt{s} = 1.296$ TeV. The upper observation (3σ) mass limits of e_8 is 777 GeV and the upper exclusion (2σ) mass limits of e_8 is 849 GeV at the LHeC-1 with $\sqrt{s} = 1.296$ TeV. These values are obtained for $L_{\text{int}} = 10$ fb^{-1} and $\Lambda = 5$ TeV. For the $\Lambda = M_{e_8}$ and $L_{\text{int}} = 10$ fb^{-1}, the statistical significances of spin-3/2 color octet electron signal at the LHeC-1 with $\sqrt{s} = 1.296$ TeV are shown in Fig. 9. It is seen from Fig. 9 that upper mass limit for discovery (5σ) of spin-3/2 color octet electron (e_8) is 1.19 TeV at the LHeC-1 with $\sqrt{s} = 1.296$ TeV. The upper observation (3σ) mass limits of e_8 is 1.21 TeV and the upper exclusion (2σ) mass limits of e_8 is 1.22 TeV at the LHeC-1 with $\sqrt{s} = 1.296$ TeV. These values are obtained for the compositeness scale $\Lambda = M_{e_8}$ and the integrated luminosity $L_{\text{int}} = 10$ fb^{-1}.
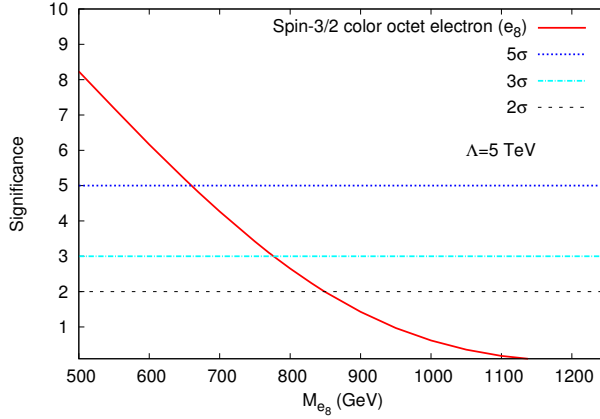
Fig. 8. The signal significances as a function of spin-3/2 color octet electron masses at the LHeC-1 with $\sqrt{s} = 1.296$ TeV. This figure is obtained for $L_{\text{int}} = 10$ fb^{-1} and $\Lambda = 5$ TeV.
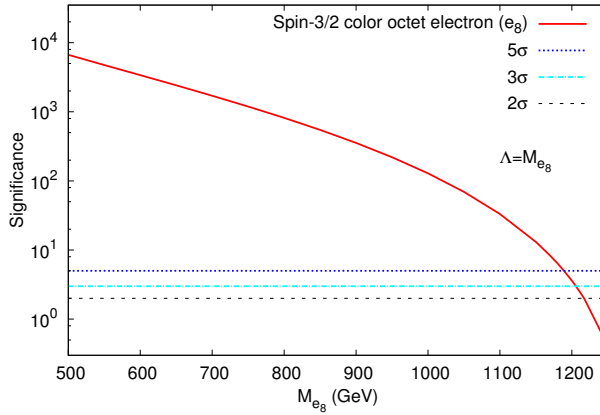

Fig. 9. The signal significances as a function of spin-3/2 color octet electron masses at the LHeC-1 with $\sqrt{s} = 1.296$ TeV. This figure is obtained for $L_{\text{int}} = 10$ fb^{-1} and $\Lambda = M_{e_8}$.

Spin-1/2 color octet electron decays into gluon- and electron-like [9, 13, 14, 16–20, 33] as spin-3/2 color octet electron. Namely, they will have the same final state in detector. In order to separate the spin-3/2 color octet electron signal from the spin-1/2 color octet electron signal, we plot normalized differential cross sections as a function of $\cos\theta$ in Fig. 10. The spin-1/2 color octet electron is produced mostly in backward direction and its minimum cross section values are in forward direction comparing to electron beam direction. However, spin-3/2 color octet electron is produced mostly in both directions (forward and backward) and its minimum cross section

values are between in -0.4 to -0.3. Therefore, the spin-3/2 color octet electron shows more different angular shape than the spin-1/2 color octet electron.
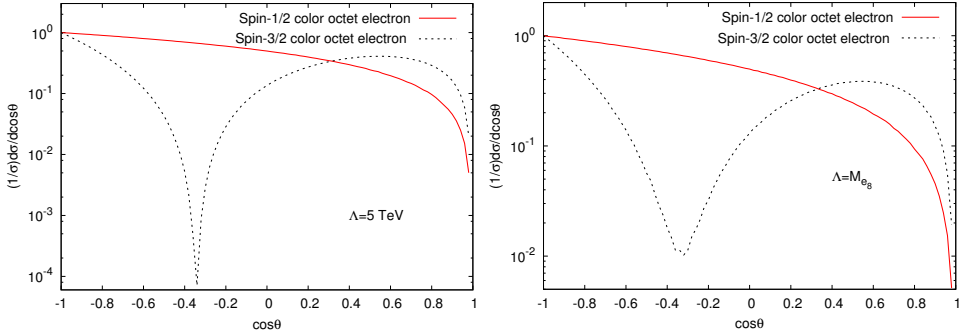

Fig. 10. Left: The differential cross section as a function of scattering angle for the spin-3/2 color octet electron ($\Lambda = 5$ TeV), and the spin-1/2 color octet electron ($\Lambda = 5$ TeV) at the LHeC-1 with $\sqrt{s} = 1.296$ TeV. Right: The differential cross section as a function of scattering angle for the spin-3/2 color octet electron ($\Lambda = M_{e_8}$), and the spin-1/2 color octet electron ($\Lambda = M_{e_8}$) at the LHeC-1 with $\sqrt{s} = 1.296$ TeV. In the both panels, spin-1/2 and spin-3/2 color octet electron mass values are taken as 500 GeV.

We have calculated the compositeness scale values for some spin-3/2 color octet masses at the LHeC-1 with $\sqrt{s} = 1.296$ TeV and $L_{\text{int}} = 10$ fb^{-1}. These values are presented as a function of spin-3/2 color octet electron masses in Fig. 11 and in Table III.
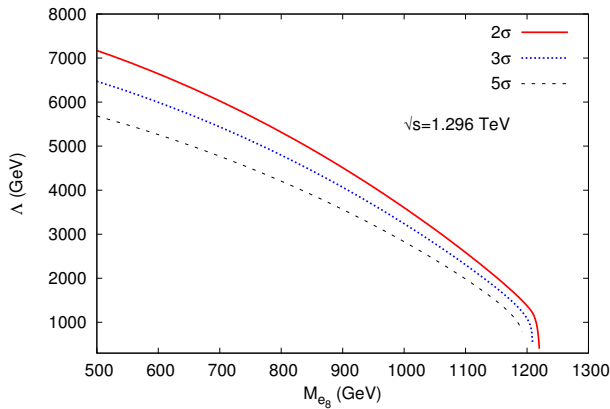

Fig. 11. Reachable values of the compositeness scale as a function of spin-3/2 color octet electron masses for the LHeC-1 with $\sqrt{s} = 1.296$ TeV and $L_{\text{int}} = 10$ fb^{-1}.

TABLE III

Reachable values of the compositeness scale for some spin-3/2 electron mass values at the LHeC-1 with $\sqrt{s} = 1.296$ TeV and $L_{\text{int}} = 10$ fb^{-1}.

M_{e_8} [GeV]	Λ [TeV]		
	5σ	3σ	2σ
500	5.68	6.47	7.17
600	5.28	6.01	6.66
700	4.80	5.47	6.07
800	4.24	4.85	5.38
900	3.61	4.13	4.59
1000	2.89	3.32	3.69
1100	2.05	2.39	2.68

It is seen from Table III that the spin-3/2 color octet electron with $M_{e_8} = 500$ GeV can be discovered up to 5.68 TeV compositeness scale value at the LHeC-1 ($\sqrt{s} = 1.296$ TeV and $L_{\text{int}} = 10$ fb^{-1}).

3.2. Higher-energy LHeC ERL
(LHeC-2 with $\sqrt{s} = 2.049$ TeV and $L_{int} = 1000$ fb^{-1})

The second option of the LHeC's center-of-mass energy is 2.049 TeV and integrated luminosity is $L_{\text{int}} = 1000$ fb^{-1}. As mentioned in previous subsection, our signal process is $ep \rightarrow e_8 \rightarrow eg + X$ and background process is $ep \rightarrow ej + X$ through γ and Z exchange, where g and j represent gluon and jet respectively, composed of quarks (u, $\bar{u}$, d, $\bar{d}$, c, $\bar{c}$, s, $\bar{s}$, b, $\bar{b}$). In order to reduce backgrounds and obtain clear signal, we need to apply some cuts. Thus, transverse momentum (P_{T}) and pseudo-rapidity (η) distributions of signal and background processes are used for determining appropriate cuts. Figure 12 presents normalized transverse momentum distributions of final state jet for signal with $\Lambda = 5$ TeV in the left panel, signal with $\Lambda = M_{e_8}$ in the right panel, and also for background (both panels). Normalized transverse momentum distributions of final state electron for signal with $\Lambda = 5$ TeV and signal with $\Lambda = M_{e_8}$, and also for background are the same as normalized transverse momentum distributions of the final state jet in Fig. 12. It is seen from left and right panels of Fig. 12 that $P_{\text{T}} > 50$ GeV cuts for the final state electron and jet essentially reduce background but signal is almost unchanged. Left and right panels in Fig. 13 represent normalized pseudo-rapidity (η) distributions of electron for signal with $\Lambda = 5$ TeV and signal with $\Lambda = M_{e_8}$, and also for background, respectively. As it is seen from left and right panels of Fig. 13, η_{e^-} distributions of signal are drastically different from η_{e^-} distributions of background. It is seen that most of the
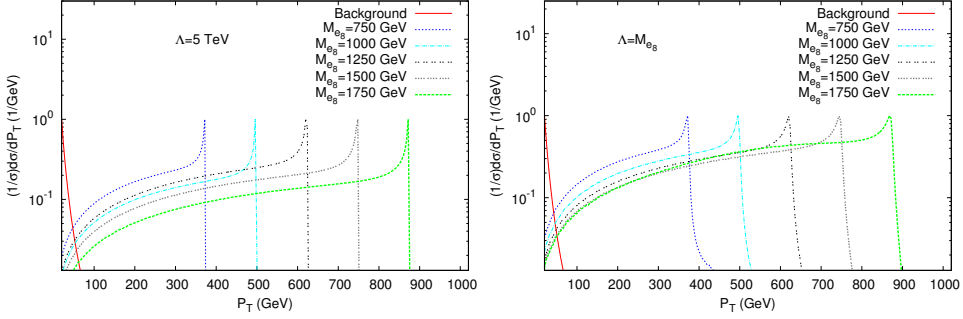
Fig. 12. Left: Normalized transverse momentum (P_T) distributions of the final state jet for signal with $\Lambda = 5$ TeV and for background at the LHeC-2. Right: Normalized transverse momentum (P_T) distributions of the final state jet for signal with $\Lambda = M_{e_8}$ TeV and for background at the LHeC-2.
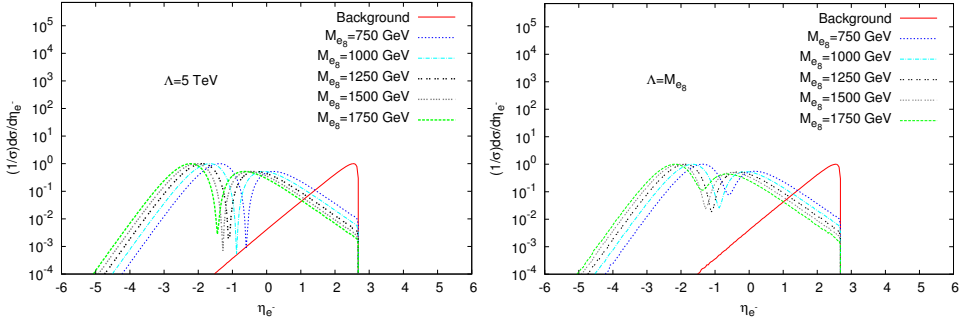

Fig. 13. Left: Normalized pseudo-rapidity distributions of final state electron for signal with $\Lambda = 5$ TeV and background at the LHeC-2. Right: Normalized pseudo-rapidity distributions of final state electron for signal with $\Lambda = M_{e_8}$ and background at the LHeC-2.

background lies in $0 < \eta_{e^-} < 3$ region in both panels of Fig. 13. Left and right panels in Fig. 14 present normalized pseudo-rapidity (η) distributions of jet for signal with $\Lambda = 5$ TeV in the left panel, signal with $\Lambda = M_{e_8}$ in the right panel, and also for background (both panels), respectively. As it is seen from Fig. 14 in both left and right panels, η_j distributions for signal and background are not drastically different. Transverse momentum (P_T) and pseudo-rapidity distributions (η) of final state jet, and electron for signal with $\Lambda = 10$ TeV give the same knowledge as transverse and pseudo-rapidity distributions of final state jet, and electron for signal with $\Lambda = 5$ TeV and $\Lambda = M_{e_8}$. Therefore, these distributions of signal with $\Lambda = 10$ TeV are not given in the text. Taking advantage of this kinematical distributions, we select pseudo-rapidity cut values as follows: $-4 < \eta_{e^-} < -0.3$ for final state

electron and $-4 < \eta_j < 2$ for final state jet. We present the invariant mass distributions for signal with $\Lambda = 5$ TeV in the left panel, signal $\Lambda = M_{e_8}$ in the right panel, and also for background (both panels) in Fig. 15.
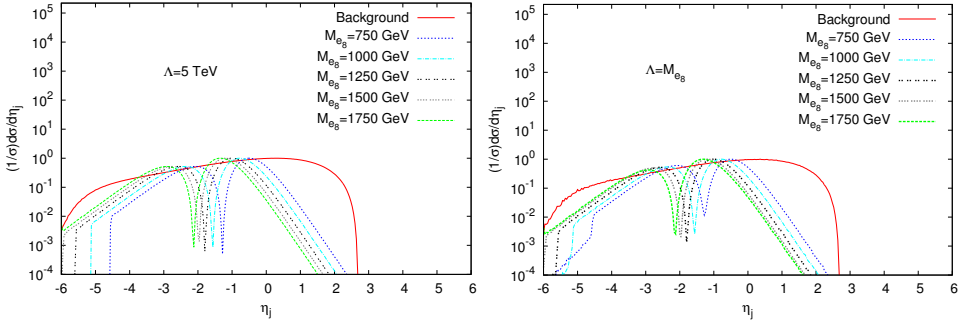

Fig. 14. Left: Normalized pseudo-rapidity distributions of final state jet for signal with $\Lambda = 5$ TeV and background at the LHeC-2. Right: Normalized pseudo-rapidity distributions of final state jet for signal with $\Lambda = M_{e_8}$ TeV and background at the LHeC-2.
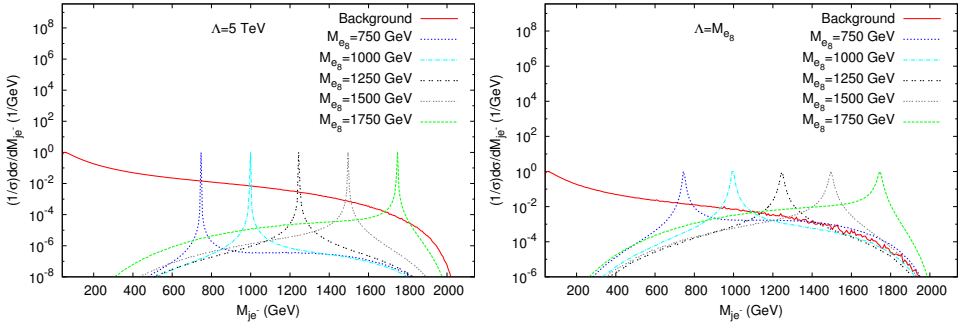

Fig. 15. Left: Normalized invariant mass distributions for signal with $\Lambda = 5$ TeV and background at the LHeC-2. Right: Normalized invariant mass distributions for signal with $\Lambda = M_{e_8}$ and background at the LHeC-2.

In order to extract the spin-3/2 color octet electron (e_8) signals for the $\Lambda = 10$ TeV, $\Lambda = 5$ TeV and $\Lambda = M_{e_8}$, and to suppress the backgrounds, we used $P_T > 50$ GeV for all final state electron and jet (these cut values are determined by Fig. 12), $-4 < \eta_{e^-} < -0.3$ for final state electron and $-4 < \eta_j < 2$ for final state jet (these cut values are determined by Figs. 13 and 14). In addition to these cut values, we have used mass window as $M_{e_8} - 10$ GeV $< M_{je^-} < M_{e_8} + 10$ GeV for signal with $\Lambda = 10$ TeV, $\Lambda = 5$ TeV and also for background. It is seen from Fig. 1 that signal decay width values are much smaller than 10 GeV for $\Lambda = 10$ TeV and $\Lambda = 5$ TeV. In addition,

we have used mass window as $M_{e_8} - 40$ GeV $< M_{je^-} < M_{e_8} + 40$ GeV for signal with $\Lambda = M_{e_8}$ and for background. It is seen from Fig. 1 that signal decay width values are approximately 20 GeV at the LHeC-2 kinematic limit (2.049 TeV) when $\Lambda = M_{e_8}$. By using this set of cuts and integrated luminosity value of the LHeC-2, $L_{\text{int}} = 1000$ fb^{-1}, we have calculated event numbers of some mass values of e_8 and the background. We present these event numbers in Table IV.

TABLE IV

The number of signal and background event for the LHeC-2 with $L_{\text{int}} = 1000$ fb^{-1}. N_{s} and N_{b} represent number of signal and background event, respectively.

M_{e_8} [GeV]	$\Lambda = 10$ TeV		$\Lambda = 5$ TeV		$\Lambda = M_{e_8}$	
	N_{s}	N_{b}	N_{s}	N_{b}	N_{s}	N_{b}
500	8.3×10^3	7.74×10^4	1.33×10^5	7.75×10^4	1.60×10^9	3.11×10^5
750	4.61×10^3	3.96×10^4	7.38×10^4	3.96×10^4	1.82×10^8	1.57×10^5
1000	2.08×10^3	1.20×10^4	3.34×10^4	1.99×10^4	2.66×10^7	7.99×10^4
1250	6.70×10^2	8.05×10^3	1.07×10^4	8.05×10^3	3.53×10^6	3.18×10^4
1500	1.19×10^2	2.07×10^3	1.89×10^3	2.07×10^3	3.04×10^5	8.33×10^3
1750	6	1.99×10^2	9.50×10^1	1.99×10^2	8.40×10^3	8.07×10^2
2000	—	—	—	—	1	—

For statistical significance, we have used Eq. (4) and presented the statistical significances of spin-3/2 color octet electron signal with $\Lambda = 10$ TeV, $\Lambda = 5$ TeV and $\Lambda = M_{e_8}$ as a function of spin-3/2 color octet electron masses in Figs. 16, 17 and 18. These figures are obtained for LHeC-2 with $\sqrt{s} = 2.049$ TeV and $L_{\text{int}} = 1000$ fb^{-1}.
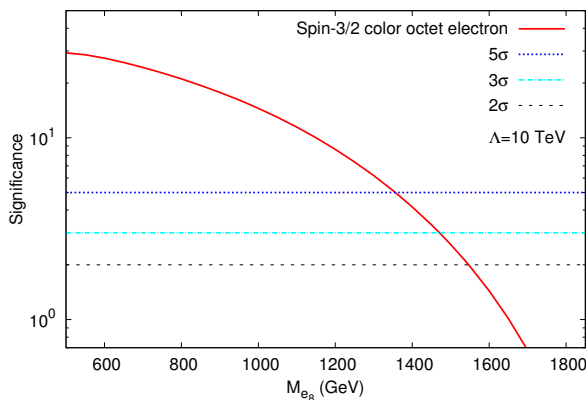

Fig. 16. The signal significances as a function of spin-3/2 color octet electron masses at the LHeC-2 with $\sqrt{s} = 2.049$ TeV. This figure is obtained for $L_{\text{int}} = 1000$ fb^{-1} and $\Lambda = 10$ TeV.

As one can see from Fig. 16, the upper mass limit for discovery (5σ) of spin-3/2 color octet electron (e_8) is 1.36 TeV at the LHeC-2 with $\sqrt{s} = 2.049$ TeV. The upper observation (3σ) mass limit of e_8 is 1.47 TeV and the upper exclusion limit of e_8 is 1.55 TeV. These upper mass values are obtained as in the case of $L_{\text{int}} = 1000$ fb^{-1} integrated luminosity and $\Lambda = 10$ TeV.

It can be seen from Fig. 17 that the upper mass limit for discovery (5σ) of spin-3/2 color octet electron (e_8) is 1.77 TeV at the LHeC-2 with $\sqrt{s} = 2.049$ TeV. The upper observation (3σ) mass limit of e_8 is 1.82 TeV and the upper exclusion limit of e_8 is 1.85 TeV. These upper mass values are obtained as in the case of $L_{\text{int}} = 1000$ fb^{-1} integrated luminosity and $\Lambda = 5$ TeV.
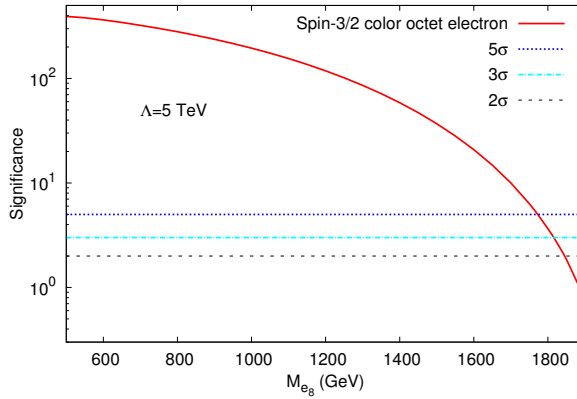

Fig. 17. The signal significances as a function of spin-3/2 color octet electron masses at the LHeC-2 with $\sqrt{s} = 2.049$ TeV. This figure is obtained for $L_{\text{int}} = 1000$ fb^{-1} and $\Lambda = 5$ TeV.
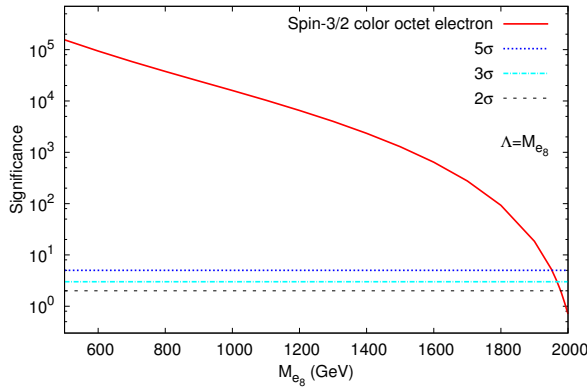

Fig. 18. The signal significances as a function of spin-3/2 color octet electron masses at the LHeC-2 with $\sqrt{s} = 2.049$ TeV. This figure is obtained for $L_{\text{int}} = 1000$ fb^{-1} and $\Lambda = M_{e_8}$ TeV.

It is seen from Fig. 18 that the upper mass limit for discovery (5σ) of spin-3/2 color octet electron (e_8) is 1.95 TeV at the LHeC-2 with $\sqrt{s} = 2.049$ TeV. The upper observation (3σ) mass limit of e_8 is 1.97 TeV and the upper exclusion limit of e_8 is 1.98 TeV. These upper mass values are obtained as in the case of $L_{\text{int}} = 1000$ fb^{-1} integrated luminosity and $\Lambda = M_{e_8}$ TeV.
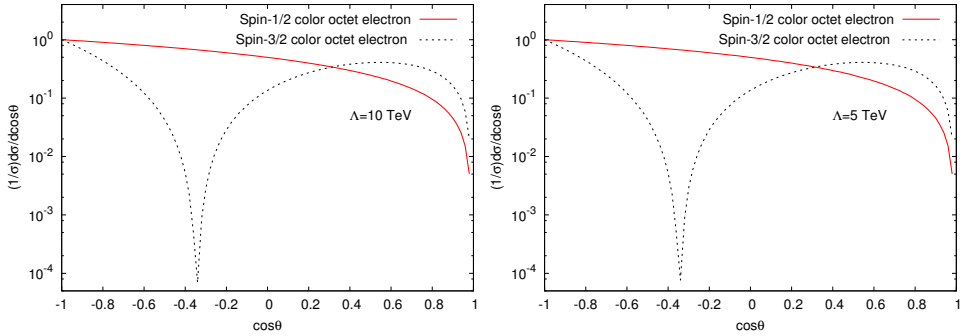

Fig. 19. Left: Differential cross sections as a function of scattering angle for the spin-3/2 color octet electron ($\Lambda = 10$ TeV), and the spin-1/2 color octet electron ($\Lambda = 10$ TeV) at the LHeC-2 with $\sqrt{s} = 2.049$ TeV. Right: Differential cross sections as a function of scattering angle for the spin-3/2 color octet electron ($\Lambda = 5$ TeV), and the spin-1/2 color octet electron ($\Lambda = 5$ TeV) at the LHeC-2 with $\sqrt{s} = 2.049$ TeV. In the both panels, spin-1/2 and spin-3/2 color octet electron mass values are taken as 1 TeV.
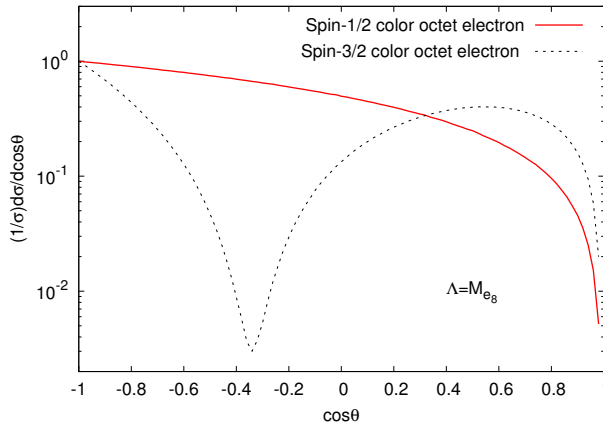

Fig. 20. Differential cross sections as a function of scattering angle for the spin-3/2 color octet electron ($\Lambda = M_{e_8}$), and the spin-1/2 color octet electron ($\Lambda = M_{e_8}$) at the LHeC-2 with $\sqrt{s} = 2.049$ TeV. The spin-1/2 and the spin-3/2 color octet electron mass values are taken as 1 TeV in our calculations.

The spin-1/2 color octet electron and the spin-3/2 color octet electron will have the same final state at the LHeC-2 with $\sqrt{s} = 2.049$ TeV. In order to diverge the spin-3/2 and the spin-1/2 color octet electron signals, we plot normalized differential cross sections as a function of $\cos\theta$ in Figs. 19 and 20. The spin-1/2 color octet electron is produced mostly in backward direction and it has its minimum cross section values in forward direction comparing to electron beam direction, whereas spin-3/2 color octet electron is produced mostly in both directions (forward and backward) and its minimum cross section values are between in -0.4 to -0.3. Therefore, the spin-3/2 color octet electron shows different angular shape from the spin-1/2 color octet electron.

In order to estimate compositeness scale for spin-3/2 color octet electron at the LHeC-2 with $\sqrt{s} = 2.049$ and $L_{\text{int}} = 1000$ fb^{-1}, we have plotted the compositeness scale as a function of spin-3/2 color octet electron masses in Fig. 21. We present reachable values of the compositeness scale for some color octet electron mass values in Table V. It can be seen from Table V that the spin-3/2 color octet electron with $M_{e_8} = 1$ TeV can be discovered up to 13.1 TeV compositeness scale value at the LHeC-2 with $\sqrt{s} = 2.049$ TeV and $L_{\text{int}} = 1000$ fb^{-1}.

TABLE V

Reachable values of the compositeness scale for some spin-3/2 electrons mass values at the LHeC-2 with $\sqrt{s} = 2.049$ TeV and $L_{\text{int}} = 1000$ fb^{-1}.

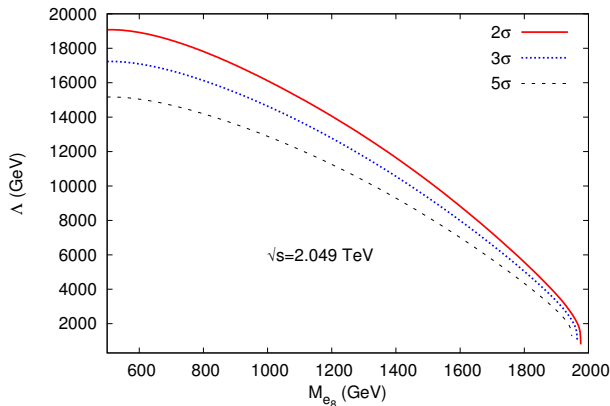| M_{e_8} [GeV]	Λ [TeV]		
	5σ	3σ	2σ
500	15.6	17.7	19.6
600	15.4	17.5	19.3
700	14.9	17.0	18.8
800	14.4	16.4	18.1
900	13.8	15.7	17.3
1000	13.1	14.9	16.5
1100	12.3	14.0	14.9
1200	11.5	13.1	14.5
1300	10.6	12.0	13.3
1400	9.6	10.9	12.0
1500	8.5	9.6	10.7
1600	7.3	8.3	9.2
1700	6.0	6.9	7.6
1800	4.6	5.3	5.9
1900	3.0	3.5	3.9

Fig. 21. Reachable values of the compositeness scale as a function of spin-3/2 color octet electron masses for the LHeC-2 with $\sqrt{s} = 2.049$ TeV and $L_{\text{int}} = 1000$ fb^{-1}.

4. Conclusion

We have performed a search for resonant production of spin-3/2 color octet electron at the LHeC. We have shown that if the compositeness scale (Λ) equals to 5 TeV, LHeC-1 with $\sqrt{s} = 1.296$ and $L_{\text{int}} = 10$ fb^{-1} will give the opportunity to discovery chance up to $M_{e_8} = 660$ GeV and observation chance up to $M_{e_8} = 777$ GeV for spin-3/2 color octet electron. In addition, LHeC-1 gives the opportunity for exclusion of spin-3/2 color octet electron up to 849 GeV. When we consider $\Lambda = M_{e_8}$ and $L_{\text{int}} = 10$ fb^{-1}case, upper mass values of the spin-3/2 color octet electron are 1.19 TeV for discovery (5σ), 1.21 TeV for observation (3σ) and 1.22 TeV for exclusion (2σ).

LHeC-2 with $\sqrt{s} = 2.049$ TeV and $L_{\text{int}} = 1000$ fb^{-1} will give the opportunity to discovery (5σ) up to $M_{e_8} = 1.36$ TeV, observation (3σ) up to $M_{e_8} = 1.47$ TeV and exclusion (2σ) up to $M_{e_8} = 1.55$ TeV for spin-3/2 color octet electron with $\Lambda = 10$ TeV. At the LHeC-2 with $\sqrt{s} = 2.049$ TeV and $L_{\text{int}} = 1000$ fb^{-1}, these upper mass values are 1.77 TeV for discovery (5σ), 1.82 TeV for observation (3σ) and 1.85 TeV for exclusion (2σ) of spin-3/2 color octet electron with $\Lambda = 5$ TeV. For spin-3/2 color octet electron with $\Lambda = M_{e_8}$, we find out that the discovery limit (5σ) is 1.95 TeV, the observation limit is 1.97 TeV and the exclusion limit is 1.98 TeV at the LHeC-2 with $\sqrt{s} = 2.049$ TeV and $L_{\text{int}} = 1000$ fb^{-1}.

We have also shown that LHeC-1 with $\sqrt{s} = 1.296$ TeV and $L_{\text{int}} = 10$ fb^{-1} will give the opportunity for discovery (5σ) of e_8 with $M_{e_8} = 500$ GeV up to $\Lambda = 5.68$ TeV. We will observe (3σ) e_8 with $M_{e_8} = 500$ GeV up to $\Lambda = 6.47$ TeV and exclude (2σ) e_8 with $M_{e_8} = 500$ GeV up to $\Lambda = 7.17$ TeV at the LHeC-1 with $\sqrt{s} = 1.296$ TeV and $L_{\text{int}} = 10$ fb^{-1} (see Table III).

LHeC-2 with $\sqrt{s} = 2.049$ TeV and $L_{\text{int}} = 1000 \text{ fb}^{-1}$ will give opportunity for discovery of e_8 with $M_{e_8} = 500$ GeV up to $\Lambda = 15.6$ TeV. We will observe e_8 with $M_{e_8} = 500$ GeV up to $\Lambda = 17.8$ TeV and exclude e_8 with $M_{e_8} = 500$ GeV up to $\Lambda = 19.6$ TeV at the LHeC-2 with $\sqrt{s} = 2.049$ and $L_{\text{int}} = 1000 \text{ fb}^{-1}$. LHeC-2 with $\sqrt{s} = 2.049$ and $L_{\text{int}} = 1000 \text{ fb}^{-1}$ will give opportunity for discovery (5σ) of e_8 with $M_{e_8} = 1$ TeV up to $\Lambda = 13.1$ TeV. We will observe e_8 with $M_{e_8} = 1$ TeV up to $\Lambda = 14.9$ TeV and exclude e_8 with $M_{e_8} = 1$ TeV up to $\Lambda = 16.5$ TeV at the LHeC-2 (see Table V).

Finally, LHeC could provide unique information about the compositeness scale (Λ) if spin-$3/2$ color octet electron masses lies within the LHeC kinematical limits.

REFERENCES

[1] G. Aad *et al.* [ATLAS Collaboration], *Phys. Lett.* **B716**, 1 (2012) [arXiv:1207.7214 [hep-ex]].

[2] S. Chatrchyan *et al.* [CMS Collaboration], *Phys. Lett.* **B716**, 30 (2012) [arXiv:1207.7235 [hep-ex]].

[3] I.A. D'Souza, C.S. Kalman, *PREONS: Models of Leptons, Quarks and Gauge Bosons as Composite Objects*, World Scientific Publishing Co., 1992.

[4] H. Harari, *Phys. Lett.* **B86**, 83 (1979).

[5] H. Fritzch, G. Mandelbaum, *Phys. Lett.* **B102**, 319 (1981).

[6] O.W. Greenberg, J. Sucher, *Phys. Lett.* **B99**, 339 (1981).

[7] R. Barbieri, R.N. Mohapatra, A. Maseiro, *Phys. Lett.* **B105**, 369 (1981).

[8] U. Baur, K.H. Streng, *Phys. Lett.* **B162**, 387 (1985).

[9] A. Celikel, M. Kantar, S. Sultansoy, *Phys. Lett.* **B443**, 359 (1998).

[10] J. Leite Lopes, J.A. Martins Simoes, D. Spehler, *Phys. Lett.* **B94**, 367 (1980); *Phys. Rev.* **D23**, 797 (1981); **D25**, 1854 (1982).

[11] Y. Tosa, R.E. Marshak, *Phys. Rev.* **D32**, 774 (1985).

[12] P. van Nieuwenhuizen, *Phys. Rep.* **68**, 189 (1981).

[13] T.G. Rizzo, *Phys. Rev.* **D33**, 1852 (1986).

[14] T.G. Rizzo, *Phys. Rev.* **D34**, 133 (1986).

[15] K.H. Streng, *Z. Phys.* **C33**, 247 (1986).

[16] J.L. Hewett, T.G. Rizzo, *Phys. Rev.* **D56**, 5709 (1997) [arXiv:hep-ph/9703337].

[17] A. Celikel, M. Kantar, *Turk. J. Phys.* **22**, 401 (1998).

[18] M. Sahin, S. Sultansoy, S. Turkoz, *Phys. Lett.* **B689**, 172 (2010) [arXiv:1001.4505 [hep-ph]].

[19] A.N. Akay, H. Karadeniz, M. Sahin, S. Sultansoy, *Europhys. Lett.* **95**, 31001 (2011) [arXiv:1012.0189 [hep-ph]].

[20] T. Mandal, S. Mitra, *Phys. Rev.* **D87**, 095008 (2013) [arXiv:1211.6394v1 [hep-ph]].

[21] The LHeC web page, http://www.lhec.org.uk

[22] J.L. Abelleira Fernandez *et al.* [LHeC Study Group], *J. Phys. G* **39**, 075001 (2012) [arXiv:1206.2913 [physics.acc-ph]].

[23] CERN-ECFA-NuPECC Workshop on the LHeC, Chavannes, Switzerland, June 2012, see http://cern.ch/lhec

[24] J.L. Abelleira Fernandez *et al.* [LHeC Study Group], arXiv:1211.4831 [hep-ex].

[25] A.N. Akay, H. Karadeniz, S. Sultansoy, *Int. J. Mod. Phys.* **A25**, 4589 (2010).

[26] https://atlas.web.cern.ch/Atlas/GROUPS/PHYSICS/ CombinedSummaryPlots/EXOTICS/ATLAS_Exotics_Summary/ ATLAS_Exotics_Summary.png

[27] https://twiki.cern.ch/twiki/pub/CMSPublic/ PhysicsResultsCombined/exo-limits_Mar2014.pdf

[28] W. Rarita, J. Schwinger, *Phys. Rev.* **60**, 61 (1941).

[29] A. Pukhov *et al.*, arXiv:hep-ph/9908288.

[30] A. Belyaev, N.D. Christensen, A. Pukhov, arXiv:1207.6082 [hep-ph].

[31] J. Pumplin *et al.*, *J. High Energy Phys.* **07**, 012 (2002); D. Stump *et al.*, *J. High Energy Phys.* **10**, 046 (2003).

[32] G.L. Bayatian *et al.* [CMS Collaboration], *J. Phys. G* **34**, 995 (2007).

[33] J. Beringer *et al.* [Particle Data Group], *Phys. Rev.* **D86**, 010001 (2012).